Soft Matter

Lateral electric field inhibits gel-to-fluid transition in lipid bilayers

Journal:	*Soft Matter*
Manuscript ID	SM-ART-06-2022-000740.R1
Article Type:	Paper
Date Submitted by the Author:	24-Jul-2022
Complete List of Authors:	Thomas, Nidhin; University of Houston Agrawal, Ashutosh; University of Houston System,

Soft Matter

ARTICLE TYPE

Cite this: DOI: 00.0000/xxxxxxxxxx

Lateral electric field inhibits gel-to-fluid transition in lipid bilayers†

Nidhin Thomas,[a] and Ashutosh Agrawal*[a]

Received Date
Accepted Date

DOI: 00.0000/xxxxxxxxxx

We report evidence of lateral electric field-induced changes in the phase transition temperatures of lipid bilayers. Our atomic scale molecular dynamics simulations show that lateral electric field increases the melting temperature of DPPC, POPC and POPE bilayers. Remarkably, this shift in melting temperature is only induced by lateral electric field, and not normal electric field. This mechanism could provide new mechanistic insights into lipid-lipid and lipid-protein interactions in the presence of endogenous and exogenous electric fields.

Introduction

Electric fields modulate the physical response of lipid membranes in both living cells and biomimetic systems. Endogenous electric fields have been shown to regulate embryonic development, wound healing, and cancer metastasis[1–4]. Epithelial cells sense electrical signals generated from disruption of epithelial layers and respond with directional migration by a process termed electrotaxis[2,4–7] in order to repair the damaged tissue. A fundamental phenomenon where electric fields interact with lipid membranes is tied to nerve excitation and propagation of action potential[8]. Neurites have been shown to grow preferentially towards the negative electrode in the presence of an applied electric field[9]. Reversible electroporation, a phenomenon in which numerous transient pores open up in plasma membrane when subjected to electric field and reseal when electric field is turned off, is routinely used to deliver drugs into cells[10,11]. Irreversible electroporation in which pores do not reseal when electric field is switched off is used to achieve cell death in cancer treatment[12–15].

Over the last several decades, experimental and modeling biophysical studies have been conducted to investigate membrane-electric field interactions. Experimental studies have revealed electric-field induced shape transformation in giant unilamellar vesicles[16–21], shape instabilities in membrane tubules[22], phase separation in multicomponent membranes[6,23], and lipid flows[24]. On the modeling front, atomistic studies[25–30] and continuum studies[31–33] have provided insights into electroporation and shape transformations in vesicles.

Despite the well characterized biological and biomedical roles of electric fields, our understanding of how cells sense and respond to electric fields is still in the formative stages. This is evident from the following example. Under the majority of the in vivo and in vitro applications discussed above, the orientation of the electric field experienced by cells or vesicles is expected to vary spatially based on the shape of the membrane. This in turn is expected to give rise to both normal and lateral (parallel) components with respect to lipid membranes. As an example, consider a vesicle subjected to a uniform electric field. Near the poles, the vesicle will experience normal electric field, and near the equatorial region, the vesicle will experience lateral electric field. However, the biophysical studies till date have predominantly analyzed the effect of normal electric fields on lipid membranes. Only a handful of biophysical studies have been performed on lateral electric field, which have demonstrated its effect on coalescence of phases[6] and buckling of membranes[30]. Furthermore, contrary to the traditional belief, normal electric fields have now been shown to be challenged in polarizing lipid membranes[31,34]. Thus, there is an impending need to investigate the consequences of lateral electric field on lipid membranes. Along this line, in this Letter, we present a new mechanism by which lateral electric field can regulate the physical response of lipid bilayers. Using atomistic studies we show, for the first time, that lateral electric field can modulate the gel-to-fluid phase transition temperature in single-component bilayers. This mechanism could potentially impact lipid-lipid and lipid-protein interactions in both living cells and biomimetic systems.

Materials and Methods

We performed all-atom simulations of flat DPPC, POPC and POPE lipid bilayers in the presence of lateral electric field. We performed the simulations in GROMACS 2018[35] with CHARMM36m[36] force field. The initial structure of the bilayers were created with 48 lipids per leaflet and 50 water molecules

[a] Department of Mechanical Engineering, University of Houston, Houston, TX, 77204, USA

* E-mail: ashutosh@uh.edu

† Electronic Supplementary Information (ESI) available: [details of any supplementary information available should be included here]. See DOI: 10.1039/cXsm00000x/

per lipid in CHARMM-GUI[37]. Periodic boundary conditions with rectangular simulation boxes were used in the simulations. Salt ions were not added as DPPC, POPC and POPE lipids are neutral and lateral electric field might have produced lateral concentration gradient of ions. We performed energy minimization using steepest descent algorithm with maximum force limit of 700 KJ/mol.nm. This was followed by three steps of NVT equilibration and three steps of NPT equilibration covering a total of 500 ps before NPT production runs. Throughout the simulation, system was maintained at fixed temperature and pressure at 1 atm. Details of the temperature of each system and total production run time is mentioned in Table S1.

During equilibration, Z-position of phosphorus atoms of lipids were constrained in order to maintain the bilayer structure till the system settled down. These constraints were gradually removed in each step of equilibration. Berendsen thermocouple[38] with 1.0 ps time constant and Berendsen semi-isotropic pressure couple with 5.0 ps time constant and 4.5 $\times 10^5$ bar $^{-1}$ compressibility were used throughout the equilibration. Nosé-Hoover thermocouple[39] and Parrinello-Rahman pressure couple[40] were used in the production run. We used Verlet cut-off scheme used throughout the simulation. Van der Waals interactions were cut-off at 1.2 nm and used force-switch vdw-modifier at 1.0 nm. Coulombic interactions were cut-off at 1.2 nm and reciprocal space interactions were calculated using PME[41]. LINCS algorithm[42] was used to constrain hydrogen bonds. External electric fields were applied in Y-direction, parallel to the bilayer surface. Production runs were performed for at least 300 ns and only last 200 ns simulation data was used to analyze the data and earlier frames were discarded as part of equilibration.

We applied Coulombic force on to the atoms to simulate electric field by prescribing 'electric fields' parameter in the 'mdp options' in GROMACS. Thus, an atom i with partial charge q_i, experienced a force $F_i = q_i E$, corresponding to an applied uniform electric field E. Annealing simulations were performed with zero external electric field and 0.075 V/nm external electric field. The lateral and normal electric field directions were selected by choosing the appropriate simulation box vectors in the mdp options. These simulations were performed at 0.05 K/ns rate. Details of the simulations are provided in Table S2. Each simulation was reproduced to verify the results.

We performed heating and cooling simulations at different electric fields to quantify the changes in the bilayer melting temperature. We obtained the starting structures for heating and cooling simulations by equilibrating bilayers at the starting temperature for at least 200 ns. Heating and cooling scans of equilibrated structures were performed with a rate of $\pm$0.05 K/ns. We chose a slow rate to ensure minimal impact on the phase transition temperature measurements. Previous atomistic simulations have shown the phase transition temperature remains constant below a heating rate of 0.3 K/ns[43]. Furthermore, our choice of a very low heating rate is also expected to reduce the thermal hysteresis observed during heating and cooling simulations[43]. We also reran the simulations with different starting structures to check the robustness of the results.

Area per lipid calculations

Area per lipid (APL) was computed by following formula.

$$APL = \frac{L_x.L_y}{N_l} \quad (1)$$

where L_x and L_y are the dimension of simulation box in X and Y direction and N_l is the number of lipids per leaflet. We used Savitzky-Golay filtering in MATLAB with third order polynomial to average the APL data over 5000 frames.

Gauche angle calculations

We used fractional gauche angle as another metric to quantify the ordering of lipid acyl chains. Dihedral angle (ϕ) '1' corresponds to C21-C22-C23-C24 carbon atoms of lipid tails. Similarly, C213-C214-C215-C216 angle of acyl tails correspond to dihedral angle '13'. 'gmx angle' command of GROMACS was used to compute the fraction of gauche angles. Gauche angle is defined as the $-60 < \phi < 60$. For equilibrium simulations, fractional gauche angle of lipid acyl tails were measured for bilayer systems at 323K and varying external electric field intensities. Phase transition of lipid bilayers in simulated annealing systems were measured by averaging individual dihedral angles per frame.

Results

We use APL as the core structural measure. Fig. 1 shows the changes in the APL with temperature while heating (red curves) and cooling (blue curves) a bilayer. The changes in the APL are represented by faint background lines but we fit a curve (solid line) to compute the effective change in the APL[43,44]. The predicted average APL of DPPC lipids is 0.53 nm^2 at 329 K in the

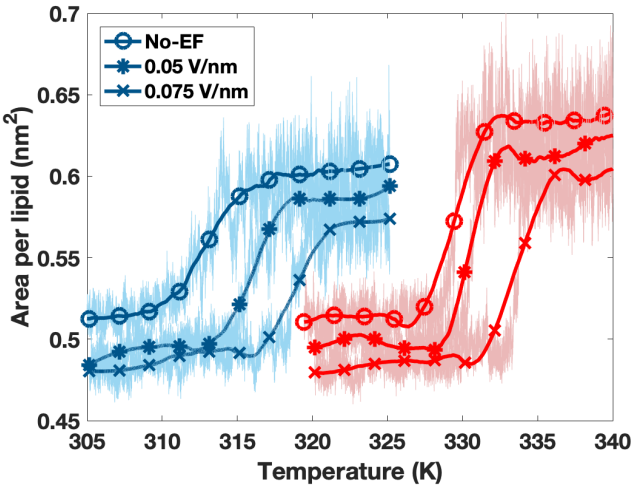

Fig. 1 Variation of area per lipid (APL) of DPPC bilayers in heating (red curves) and cooling (blue curves) simulations. The discrete jumps in the red curves depict a first-order phase transition from gel phase to fluid phase. Presence of lateral electric field shifts the discrete jumps rightward, delaying the gel-to-fluid transition. The cooling curves show similar rightward shifts in phase transition temperatures. The relative shifts in the heating and cooling curves show hysteresis emerging from longer time scale associated with disordered state to ordered state transition.

absence of the electric field. This value agrees with an earlier estimate[43], and suggests that the bilayer is in the gel phase. When we increase the temperature to 329.6 K, the APL increases to 0.62 nm^2. This increase in the APL implies that the bilayer has become fluid and undergone phase transition. The discrete jump observed in the APL curve indicates that the bilayer underwent a first-order phase transition.

When we subject the bilayer to an electric field of 0.05 V/nm, the APL increases from 0.53 nm^2 to 0.61 nm^2 at 330.5 K. When we apply a higher electric field of 0.075 V/nm, the APL jumps from 0.53 nm^2 to 0.60 nm^2 at 333.9 K. Thus, the lateral electric fields shift the melting temperature by 1.0 K and 4.5 K for the DPPC bilayer. Fig. 2a shows the DPPC bilayer at 333 K in the absence of the electric field. The bilayer is in the fluid phase and has a thickness of 4.0 nm. Fig. 2b shows the bilayer at the same temperature but in the presence of 0.075 V/nm lateral electric field. The lipid acyl chains become straighter and the bilayer thickness increases to 4.4 nm as the bilayer is in the gel phase because of delayed melting induced by the electric field. We would like to note that the observed changes in the tilt of the lipid acyl chains with respect to bilayer normal and apparent shifts of headgroups occur due to phase transition, and not specifically because of the applied electric field. Similar structural changes have been observed in lipid bilayers undergoing gel-phase transition in the absence of electric field[43–45].

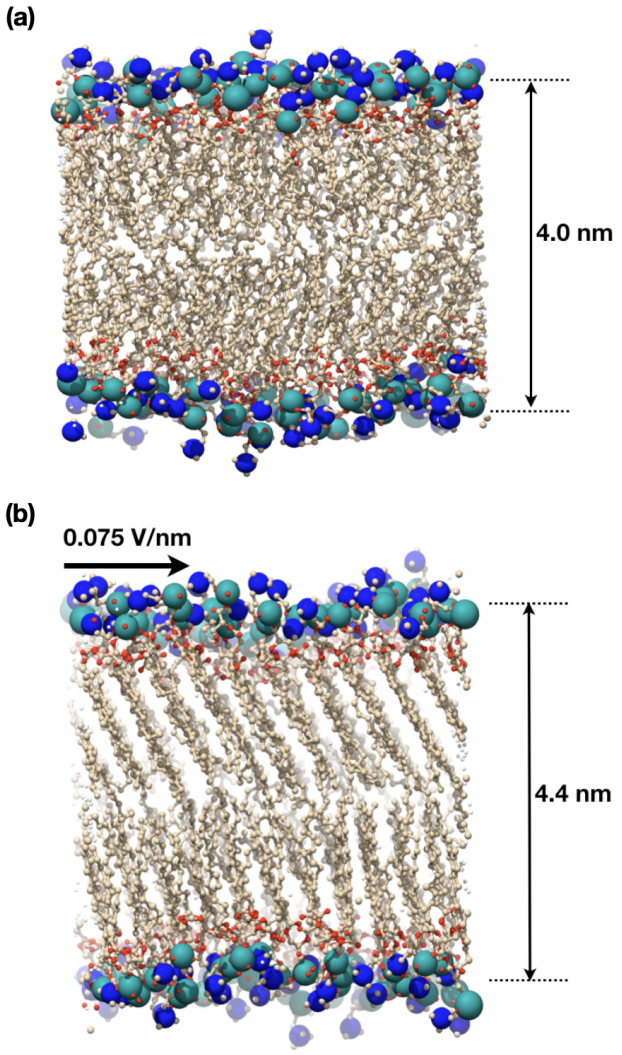

Fig. 2 DPPC bilayer at 330 K in the absence and presence of electric field. (a) DPPC bilayer is in the fluid phase in the absence of the applied electric field. The acyl chains are disordered and the bilayer has a thickness of 4 nm. (b) The bilayer is in the gel phase at the same temperature in the presence of a lateral electric field of 0.075 V/nm. The lipids are straighter and the bilayer thickness is increases to 4.4 nm.

The reverse transition curves obtained from cooling simulations are shifted to lower melting temperatures and show hysteresis. Phase transition occurs at 312.6 K, 316.2 K and 318.8 K, respectively for 0 V/nm, 0.05 V/nm and 0.075 V/nm electric fields. The shifted transition temperatures and the hysteresis occur because the process of ordering from a disordered state occurs on a slower time scale compared to the process of disordering from an ordered state. Such thermal hysteresis has been reported in the literature by both experimental studies[46,47] and simulation studies[43]. While gel-to-fluid transition occurs via a one-step process, fluid-to-gel transition has been shown to get trapped in ripple-like phases creating hysteresis[43]. Because of this difference in the time scales associated with the heating and the cooling simulations, heating runs provide a more accurate quantitative measure of the phase transition boundaries. Nonetheless, cooling runs provide a qualitative validation of the results.

To verify our findings further, we computed the fraction of the acyl chain gauche dihedrals as the second structural measure. The gauche angle is the fraction of the dihedral angle of acyl chain carbon atoms(ψ) which are within -60 and 60, computed directly from GROMACS. Fig. 3 shows the evolution of the fraction of the gauche angle with temperature. At lower temperatures, the DPPC membrane has a small fraction of gauche angle indicating the gel phase with acyl chains in the *trans* configuration. As the temperature increases, the ordered lipid acyl chains start to melt and undergo gauche rotational isomerization. As a result, the fraction

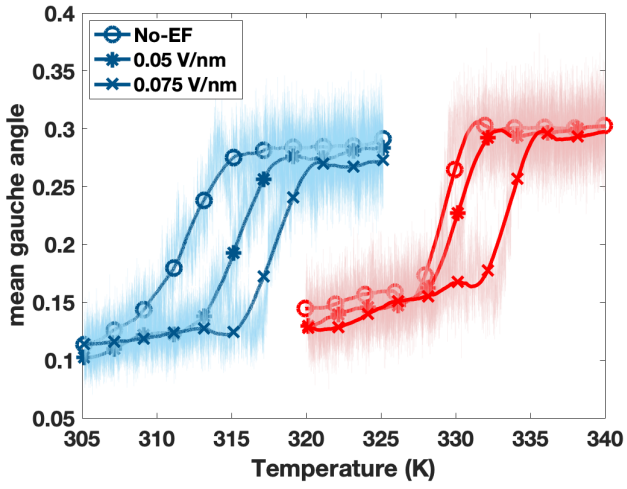

Fig. 3 Fraction of gauche angle of acyl chains in the DPPC bilayer. The heating (red curves) and cooling (blue curves) calculations confirm the electric-field induced shifts in the phase transition temperature.

undergoes a jump at the phase transition temperature confirming the predictions revealed by the APL plots. The heating plots show phase transition at 329.5 K and 333.5 K for 0 V/nm and 0.075 V/nm. A jump in the gauche angle can also be observed in the cooling simulations. Fig. 3 also shows the hysteresis behaviour during the heating and the cooling simulations confirming the first-order phase transition in DPPC bilayers.

Having confirmed the effect of lateral electric on DPPC bilayers, we simulated its effect on two other key lipids: 1-palmitoyl-2-oleoyl-sn-glycero-3-phosphocholine (POPC) and 1-palmitoyl-2-oleoyl-sn-glycero-3-phosphoethanolamine (POPE). Fig. 4 shows the APL plots as a function of temperature and electric field. The APL increases from 0.54 nm^2 to 0.63 nm^2 at 275 K temperature for the POPC bilayer in the absence of the electric field. After subjecting the bilayer to an electric field of 0.075 V/nm, the APL increased from 0.52 nm^2 to 0.60 nm^2 at 288 K. Thus, the lateral electric field induces a 13 K shift in the phase transition temperature of the POPC bilayer. Similarly, for POPE bilayer, the APL increases from 0.49 nm^2 to 0.59 nm^2 at 316 K in the absence of the electric field. In the presence of 0.075 V/nm electric field, the APL increases from 0.48 nm^2 to 0.58 nm^2 at 332 K. Thus, the lateral electric field shifts melting temperature by 16 K for the POPE bilayer. These results demonstrate that lateral electric field affects a wide variety of lipids. They also show that the effect of lateral electric field is different for different lipid types. The shifts obtained for the POPC and POPE bilayers are much larger than that obtained for DPPC bilayer. These predictions for the three lipid systems are confirmed by repeated simulations with different starting structures presented in Figs. S1 and S2.

Discussion

Endogenous and exogenous electric fields play a critical role in growth and repair of cells and tissues. In this study, we present a new mechanism by which electric fields can control the physical response of cellular membranes. Our findings show that lateral electric fields can regulate the phase transition in lipid bilayers in lipid-dependent manner. This finding is qualitatively aligned with the recent study that shows that the lateral dielectric coefficient is magnified in the head group region that influences head group ordering[48]. As cellular membranes invariably have heterogeneous lipid composition and electric fields possess spatial variations, cellular membranes can have a heterogeneous distribution of gel and fluid phases. This electric-field dependent property can contribute to the directional response of cells in the presence of electric fields. Our findings lend support to the soliton theory of nerve impulse propagation[49,50] which relies on local phase changes in lipid membrane. In fact, electric field-induced regulation of lipid phase could also potentially modulate the gating of voltage-sensitive ion channels in neurons.

We can understand the electric field-induced phase changes by its impact on the bilayer structure. Lateral electric field reorients the P-N dipoles in the lipid headgroups. This generates an in-plane polarization in the bilayer. According to a recent electromechanical theory[31], the in-plane polarization generated by

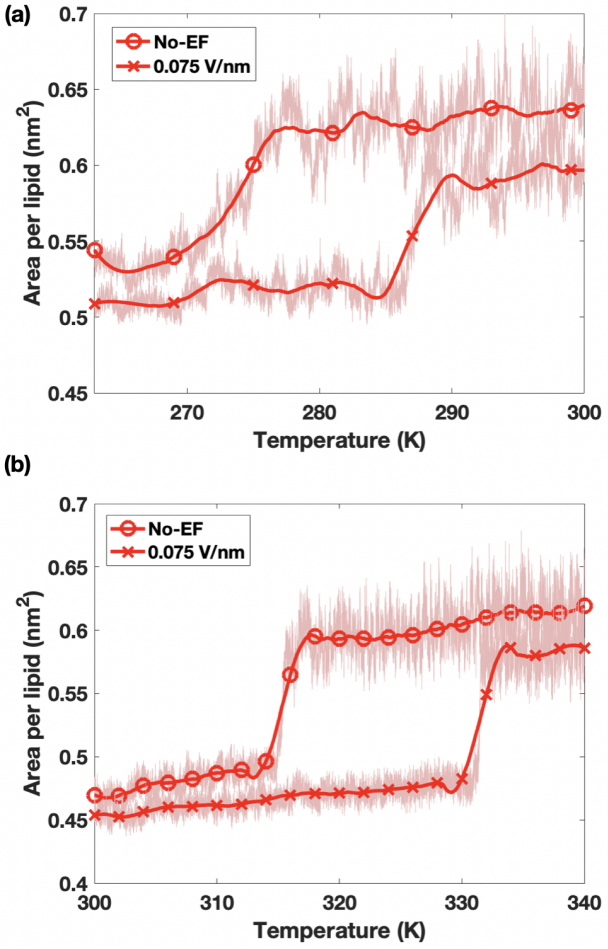

Fig. 4 Variation of area per lipid (APL) of POPC (a) and POPE (b) bilayers during heating simulations. The curves in the presence of electric field show significant rightward shifts in the phase transition temperatures.

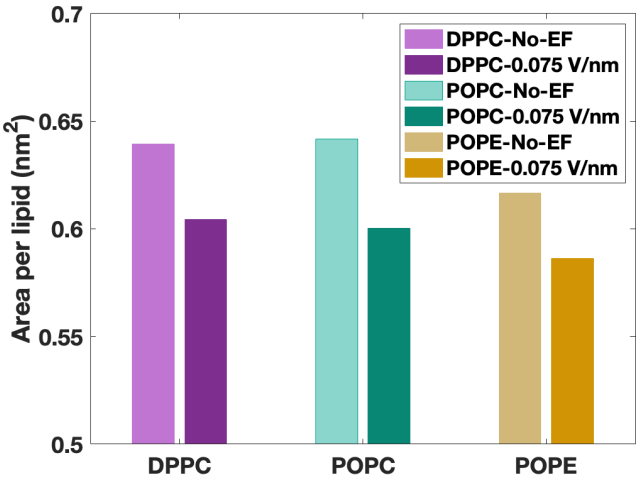

Fig. 5 Lateral electric field reduces the APL of the bilayer systems in the fluid phase. Despite being in the same phase, bilayers with and without electric field have different APLs. This change is a consequence of in-plane compression generated in the bilayer by the lateral electric field.

a tangential electric field generates a compressive stress in a bilayer. This compressive stress in turn would shift the gel-to-fluid phase transition to a higher temperature. The inhibition of gel-to-fluid transition by compressive stress has been demonstrated in previous atomistic studies[51,52]. The presence of compressive stress in the bilayer is also confirmed by Fig. 5 which shows the APL of the three lipids in the fluid phase. The histograms in the presence of electric field are shorter than the those in the absence of electric field. Thus, despite being in the same phase, the lipids have smaller APLs in the presence of an electric field indicating the existence of compressive stress in the bilayers. This finding is supported by a previous atomistic study that has shown buckling of a flat bilayer in the presence of a lateral electric field[30]. In addition, this paper also showed that higher electric field is needed to eletroporate bilayer in the presence of lateral electric field. This effect could possibly occur because of stiffening of the bilayer caused by areal compression (and resulting thickening) induced by lateral electric field. The fact that electroporation preferably occurs in fluid phase with lower stiffness compared to gel-phase has also been experimentally demonstrated[23].

Some remarks are in order with regards to the numerical approach. First, the phase transition temperature of a lipid bilayer depends on the choice of force field used in the atomistic simulations. For a DPPC bilayer, the phase transition temperature falls in the range of 312 K to 343 K depending on the force field used[43–45]. These numerical values can differ from the experimental estimates of $\sim$315.0 K for DPPC bilayer[53–55]. Second, the electric field values used in the atomistic studies are in the range of 0.05-10.2 V/nm[25–29]. The electric fields used in the experiments typically are on the order of 10^{-3} V/nm[23,56,57] but may reach a value as high as 0.08 V/nm[58]. The typical difference between the electric field values in simulations and experiments likely arises from the fact that the numerical studies are performed in an idealized system lacking multiple lipid species, heterogeneities and ionic concentrations. While such quantitative differences exist between simulations and experiments, numerical studies have been instrumental in providing molecular insights into phase behavior and electric-field response of lipid membranes. The robustness of the predictions in this study, for example, is illustrated by comparing heating and cooling simulations. Despite a shift in the absolute phase transition temperatures predicted by the two pathways, the relative electric field-induced phase transition shifts they predict remain very similar. Thus, absolute shifts in the phase transition temperature created by transient entrapment in the energy wells during cooling simulations do not compromise the ability of lateral electric field to modulate lipid bilayers. A similar argument could be extended for the differences that arise from a choice of molecular force fields. Third, the absence of salt in the buffer solution in the systems discussed above do not compromise the validity of our results. To verify this, we simulated the DPPC system with 0.150 M KCl in the aqueous buffer. Fig. S3 shows the APL plots for the heating simulations. Presence of salt leads to $\sim$ 1 K change in the absolute values of the phase transition temperatures with and without electric field, leaving the electric-field induced shift in the phase transition unaffected.

Finally, we would like to emphasize that the phase change presented in this study is only induced by lateral electric field. Application of normal electric field does not lead to any noticeable shift in the phase transition temperatures. Fig. S4 shows the heating and cooling simulations for DPPC lipids in the presence of 0 V/nm and 0.075 V/nm electric field perpendicular to the bilayer. The two sets of plots almost overlap showing no shifts in the meting temperature. Overall, these findings reveal a need to disentangle the roles of normal and lateral electric fields, and further investigate the biophysical underpinnings of the electromechanical behaviour of cellular membranes.

Author Contributions

A.A. conceived the study. N.T. and A.A. designed the MD simulations, analyzed the data and wrote the manuscript. N.T. carried out the MD simulations.

Competing interests

The authors declare no competing interests.

Acknowledgments

A.A. acknowledges support from NSF Grants CMMI-1727271 and CMMI-1931084. The authors acknowledge the use of the Opuntia, Sabine, and Carya clusters to perform the simulations and the advanced technical support from the Research Computing Data Core at UH to carry out the research presented here.

Notes and references

1 R. Nuccitelli, *Radiation protection dosimetry*, 2003, **106**, 375–383.
2 R. Nuccitelli, *Current topics in developmental biology*, 2003, **58**, 1–26.
3 M. Zhao, Seminars in cell & developmental biology, 2009, pp. 674–682.
4 M. E. Mycielska and M. B. Djamgoz, *Journal of cell science*, 2004, **117**, 1631–1639.
5 M. Zhao, J. Pu, J. V. Forrester and C. D. McCaig, *The FASEB Journal*, 2002, **16**, 857–859.
6 B.-j. Lin, S.-h. Tsao, A. Chen, S.-K. Hu, L. Chao and P.-h. G. Chao, *Proceedings of the National Academy of Sciences*, 2017, **114**, 8568–8573.
7 G. Tai, M. Tai and M. Zhao, *Burns & trauma*, 2018, **6**, year.
8 L. Squire, D. Berg, F. E. Bloom, S. Du Lac, A. Ghosh and N. C. Spitzer, *Fundamental neuroscience*, Academic press, 2012.
9 L. Hinkle, C. McCaig and K. Robinson, *The Journal of physiology*, 1981, **314**, 121–135.
10 A. Polak, M. Tarek, M. Tomšič, J. Valant, N. P. Ulrih, A. Jamnik, P. Kramar and D. Miklavčič, *Bioelectrochemistry*, 2014, **100**, 18–26.
11 T. Kotnik, P. Kramar, G. Pucihar, D. Miklavcic and M. Tarek, *IEEE Electrical Insulation Magazine*, 2012, **28**, 14–23.
12 N. Jourabchi, K. Beroukhim, B. A. Tafti, S. T. Kee and E. W. Lee, *Gastrointestinal Intervention*, 2014, **3**, 8–18.
13 T. B. Napotnik, T. Polajzer and D. Miklavcic, *Bioelectrochemistry*, 2021, **141**, 107871.

14 K. N. Aycock and R. V. Davalos, *Bioelectricity*, 2019, **1**, 214–234.

15 A. Gothelf, L. M. Mir and J. Gehl, *Cancer treatment reviews*, 2003, **29**, 371–387.

16 R. Dimova, N. Bezlyepkina, M. D. Jordö, R. L. Knorr, K. A. Riske, M. Staykova, P. M. Vlahovska, T. Yamamoto, P. Yang and R. Lipowsky, *Soft Matter*, 2009, **5**, 3201–3212.

17 P. M. Vlahovska, R. S. Gracia, S. Aranda-Espinoza and R. Dimova, *Biophysical journal*, 2009, **96**, 4789–4803.

18 K. A. Riske and R. Dimova, *Biophysical journal*, 2005, **88**, 1143–1155.

19 P. M. Vlahovska, *Soft matter*, 2015, **11**, 7232–7236.

20 R. Dimova, K. A. Riske, S. Aranda, N. Bezlyepkina, R. L. Knorr and R. Lipowsky, *Soft matter*, 2007, **3**, 817–827.

21 J. Steinkühler, J. Agudo-Canalejo, R. Lipowsky and R. Dimova, *Biophysical journal*, 2016, **111**, 1454–1464.

22 K. P. Sinha, S. Gadkari and R. M. Thaokar, *Soft Matter*, 2013, **9**, 7274–7293.

23 D. L. Perrier, L. Rems, M. T. Kreutzer and P. E. Boukany, *Scientific reports*, 2018, **8**, 1–10.

24 M. Staykova, R. Lipowsky and R. Dimova, *Soft Matter*, 2008, **4**, 2168–2171.

25 D. P. Tieleman, H. Leontiadou, A. E. Mark and S.-J. Marrink, *Journal of the American Chemical Society*, 2003, **125**, 6382–6383.

26 C. Zhou and K. Liu, *Biomedical engineering online*, 2019, **18**, 1–16.

27 A. Polak, D. Bonhenry, F. Dehez, P. Kramar, D. Miklavčič and M. Tarek, *The Journal of membrane biology*, 2013, **246**, 843–850.

28 L. Delemotte and M. Tarek, *The Journal of membrane biology*, 2012, **245**, 531–543.

29 M. Tarek, *Biophysical journal*, 2005, **88**, 4045–4053.

30 F. Castellani, J. Teissié and P. Vernier, *The Journal of membrane biology*, 2018, **251**, 229–236.

31 D. Steigmann and A. Agrawal, *Mathematics and Mechanics of Complex Systems*, 2016, **4**, 31–54.

32 L.-T. Gao, X.-Q. Feng, Y.-J. Yin and H. Gao, *Journal of the Mechanics and Physics of Solids*, 2008, **56**, 2844–2862.

33 P. F. Salipante and P. M. Vlahovska, *Soft matter*, 2014, **10**, 3386–3393.

34 N. Thomas and A. Agrawal, *EPL (Europhysics Letters)*, 2021, **134**, 68003.

35 M. J. Abraham, T. Murtola, R. Schulz, S. Páll, J. C. Smith, B. Hess and E. Lindahl, *SoftwareX*, 2015, **1**, 19–25.

36 J. Huang, S. Rauscher, G. Nawrocki, T. Ran, M. Feig, B. L. de Groot, H. Grubmüller and A. D. MacKerell, *Nature methods*, 2017, **14**, 71–73.

37 J. Lee, X. Cheng, J. M. Swails, M. S. Yeom, P. K. Eastman, J. A. Lemkul, S. Wei, J. Buckner, J. C. Jeong, Y. Qi *et al.*, *Journal of chemical theory and computation*, 2016, **12**, 405–413.

38 H. J. Berendsen, J. v. Postma, W. F. van Gunsteren, A. DiNola and J. R. Haak, *The Journal of chemical physics*, 1984, **81**, 3684–3690.

39 S. Nosé, *The Journal of chemical physics*, 1984, **81**, 511–519.

40 M. Parrinello and A. Rahman, *Journal of Applied physics*, 1981, **52**, 7182–7190.

41 T. Darden, D. York and L. Pedersen, *The Journal of chemical physics*, 1993, **98**, 10089–10092.

42 B. Hess, H. Bekker, H. J. Berendsen and J. G. Fraaije, *Journal of computational chemistry*, 1997, **18**, 1463–1472.

43 L. Sun and R. A. Böckmann, *European Biophysics Journal*, 2018, **47**, 151–164.

44 B. Kowalik, T. Schubert, H. Wada, M. Tanaka, R. R. Netz and E. Schneck, *The Journal of Physical Chemistry B*, 2015, **119**, 14157–14167.

45 K. Pluhackova, S. A. Kirsch, J. Han, L. Sun, Z. Jiang, T. Unruh and R. A. Böckmann, *The Journal of Physical Chemistry B*, 2016, **120**, 3888–3903.

46 J. H. Davis, *Biophysical journal*, 1979, **27**, 339–358.

47 S. Black and G. Dixon, *Biochemistry*, 1981, **20**, 6740–6744.

48 P. Loche, C. Ayaz, A. Wolde-Kidan, A. Schlaich and R. R. Netz, *The Journal of Physical Chemistry B*, 2020, **124**, 4365–4371.

49 T. Heimburg and A. D. Jackson, *Proceedings of the National Academy of Sciences*, 2005, **102**, 9790–9795.

50 E. V. Vargas, A. Ludu, R. Hustert, P. Gumrich, A. D. Jackson and T. Heimburg, *Biophysical Chemistry*, 2011, **153**, 159–167.

51 X. Kong, S. Qin, D. Lu and Z. Liu, *Physical Chemistry Chemical Physics*, 2014, **16**, 8434–8440.

52 S. Katira, K. K. Mandadapu, S. Vaikuntanathan, B. Smit and D. Chandler, *Elife*, 2016, **5**, e13150.

53 D. Marsh, *Chemistry and physics of lipids*, 1991, **57**, 109–120.

54 W. Chen, F. Duša, J. Witos, S.-K. Ruokonen and S. K. Wiedmer, *Scientific reports*, 2018, **8**, 1–11.

55 L. Redondo-Morata, M. I. Giannotti and F. Sanz, *Langmuir*, 2012, **28**, 12851–12860.

56 A. R. Thiam, N. Bremond and J. Bibette, *Physical review letters*, 2011, **107**, 068301.

57 E. C. Gianulis, J. Lee, C. Jiang, S. Xiao, B. L. Ibey and A. G. Pakhomov, *Scientific reports*, 2015, **5**, 1–10.

58 A. Hemmerle, G. Fragneto, J. Daillant and T. Charitat, *Physical review letters*, 2016, **116**, 228101.